A High-speed Tunable Optical Filter Using a Semiconductor Ring Resonator

Shinji Matsuo[†], *Yoshitaka Ohiso, and Toru Segawa*

Abstract

A high-speed tunable optical filter incorporating a semiconductor ring resonator is a key device in photonic packet switching. To achieve a wide tuning range we designed a double-ring structure, in which two ring resonators are connected in series, and fabricated it using the InGaAsP-InP material system. This device exhibits a total free spectral range (FSR) of 1.7 THz and contrast ratio of 9.5 dB. The ring radii are 25.2 and 17.8 μm, which correspond to FSRs of 340 and 425 GHz, respectively. The switching time of the device is 2.5 ns.

1. Introduction

The wavelength division multiplexing (WDM) transport network has emerged as the best way to make the large-capacity networks needed for future Internet traffic. In such a network, photonic packet switches are expected to offer high-throughput switching because they are based on optical technologies for long-haul transmission. Several photonic packet switches using WDM technologies have been proposed. In many of the systems using them, a high-speed tunable optical filter is a key device because optical packets with different wavelengths must be selected packet by packet [1], [2]. In those reports, the filters were fabricated by integrating the arrayed waveguide grating (AWG) filters and semiconductor optical amplifier (SOA) gate switches. Although they exhibited low insertion loss, low crosstalk, and high-speed-switching, they seem likely to be expensive because they require many components.

Optical ring resonators are very useful for optical filters, and it should be possible to fabricate them at a low cost because of their simple structure. Recently, semiconductor ring or microdisk resonators with a free spectral range (FSR) of more than 20 nm have been demonstrated for GaAs-AlGaAs and InGaAsP-InP material systems [3], [4]. However, when current injection is used for high-speed tuning of the resonant wavelength, the tuning range is limited to a few nanometers to prevent thermal effects. To overcome this problem, we used a double-ring structure in which two single-ring resonators with different FSRs are connected in series: we call this a double-ring resonator. In this paper, we describe a large-capacity photonic packet switch using a tunable optical filter and the fabrication of a high-speed tunable optical filter using the ring resonator.

† NTT Photonics Laboratories
Atsugi-shi, 243-0198 Japan
E-mail: mash@aecl.ntt.co.jp

2. Large-capacity photonic packet switch using WDM technology

2.1 Configuration of the large-capacity switch using the photonic switch

The most important problems to be solved are the limited scalability of the optical buffer and the competition control of the packets because while light can be switched quickly, it is hard to buffer. Furthermore, when some functions are implemented optically, they will need complicated optical circuits because the logic functions are poor. To overcome these problems, one group designed a high-throughput switch using the features of both photonic and electrical switches efficiently [5]. The required number of optical buffers could be reduced by complementing optical buffers with electrical buffers. However, a fiber delay line used as an optical buffer was required for every output port because the optical buffer was connected to the latter part of the optical switching block.

Thus, many fiber delay lines were needed in the switching fabric.

In this paper, we describe a photonic packet switch using the high-speed tunable optical filter with fewer fiber delay lines. Figure 1 shows a schematic diagram of the switch. It consists of the photonic packet switch, consisting of the optical buffer and the optical switch, and many electrical routers. The photonic packet switch switches the input packets to corresponding electrical routers.

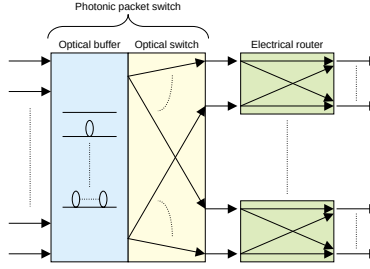

Fig. 1. Schematic diagram of the switch.

2.2 Configuration of the photonic packet switch

Figure 2 shows the configuration of the photonic packet switch. The optical buffer consists of optical couplers, fiber delay lines, fiber amplifiers, and high-speed wavelength selectors. The fiber delay lines have different lengths to achieve different buffering times. The optical switch consists of an optical coupler and several high-speed tunable optical filters.

An input packet is converted to the wavelength for that input port at a wavelength converter. The optical coupler divides the optical power of input packets entering the fiber delay lines. Since each wavelength converter changes the input packet to a different wavelength, the input packets are multiplexed without wavelength collision at the optical coupler. Therefore, all input ports can share one fiber delay line. This means that the optical buffer has just one set of fiber delay lines for the whole photonic packet switch. The wavelength selector is connected to the output port of each fiber delay line. It must select

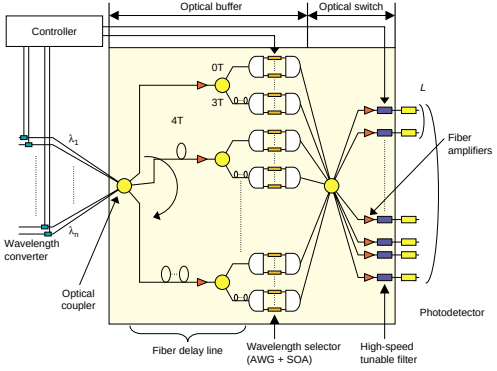

Fig. 2. Configuration of the photonic packet switch.

many wavelengths simultaneously from the multiplexed input packets because the required delay time must be set independently for each input packet. For this reason, we considered using the combination of AWG filters and SOA gates as a wavelength selector [6]. In this optical buffer, the packets can be selected with any desired delay time (i.e., random access memory). This avoids head of line blocking, which causes a problem with input-buffer-type switches. In this optical switch, packets that have the same wavelength and different delay time are not output to the optical switch part in the same time slot, so one input port transmits one packet in one time slot to the optical switch part. Thus, the packets selected by the wavelength selectors are distributed to all output ports by the optical coupler. Therefore, this optical switch part operates as a non-blocking broadcast-and-select optical switch, in which the input packets are filtered by the high-speed wavelength tunable filter placed in front of each output port.

2.3 Effect of speeding up photonic packet switching

We estimated the packet-loss probability characteristics of the optical buffer part for various numbers L of tunable filters and photodetectors for one output port. Figure 3 shows the calculation results. Note that although the dividing number of the optical coupler in the optical switch part is multiplexed by L, the optical buffer part does not change. We assumed that the load p was 0.8, the switch size N was infinite, and packet arrivals were random. We also assumed that the optical buffer was a first-in first-out (FIFO) buffer to simplify the calculation. To obtain a packet loss probability of less than 10^{-12}, we need 10 optical buffers when L is 3. As shown in this figure, speeding up the optical switch by increasing L has the great advantage of reducing the number of optical buffers. As explained before, since our optical buffer is a random access memory, the required number of buffers is small even if we assume traffic is bursty.

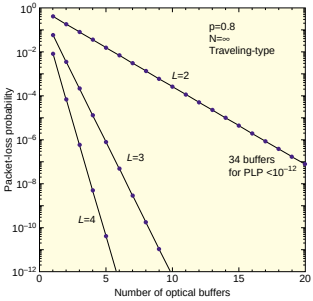

Fig. 3. Packet-loss probability characteristics of the optical buffer part for various numbers of tunable filters and photodetectors for one output port.

The problem with this solution is, of course, the increase in the number of tunable filters and photodetectors. Thus, it is very important to make a low-cost high-speed tunable optical filter. Our high-speed wavelength tunable filter using a semiconductor ring resonator will reduce the cost.

3. Device structure and fabrication of tunable filter using the ring resonator

3.1 Operating principle

Optical ring resonators are very useful for optical filters and it should be possible to fabricate them at low cost because of their simple structure. In a ring resonator, the resonant wavelength can be controlled by controlling the refractive index of the ring waveguide. When the ring waveguide's length is l and its effective refractive index is n_{eff}, the resonant wavelength λ_0 is given by

$$\lambda_0 = \frac{n_{eff} l}{m} , \quad (1)$$

where m is an integer. The FSR is given by

$$FSR = \frac{c_0}{n_{eff} l} , \quad (2)$$

where c_0 is the speed of the light in vacuum. From (1), the change in resonant wavelength $\Delta\lambda$ is given by

$$\Delta\lambda = \frac{\Delta n_{eff} l}{m} , \quad (3)$$

where Δn_{eff} is the change in effective refractive index in the ring waveguide. From (1) and (3), we obtain

$$\frac{\Delta\lambda}{\lambda_0} = \frac{\Delta n_{eff}}{n_{eff}} . \quad (4)$$

Equation (4) shows that the wavelength change of the ring resonator is independent of the *FSR*, *l*, and *m* and depends on the effective refractive index change.

In the photonic packet switch, the switching time of the tunable filter must be less than a few nanoseconds. We can achieve this by controlling the effective refractive index change using the applied voltage or injection current on a semiconductor. The effective refractive index change produced by the applied voltage is as small as 0.1%, although it does provide a fast switching time of less than 100 ps. Therefore, we chose the current injection effect in semiconductors, although its refractive-index change is still only 0.3%. However, when the current injection is increased, heat is generated. This causes the refractive index to change on the order of milliseconds, so the selected wavelength (i.e., the resonant wavelength set by the current injection) changes gradually. Thus, the wavelength tunable range of one ring resonator must be restricted to a few nanometers to avoid this thermal effect.

3.2 Structure of double ring resonator

To overcome these problems, we use the double ring structure [7], [8]. Figure 4 is a schematic of our double ring resonator. The filter consists of two ring resonators R1 and R2, each with different FSRs, to achieve a wide tuning range. Each ring resonator is coupled with the straight waveguide via an optical coupler. In this device, input WDM signals, which have resonant frequencies of ring resonator R1, pass through R1 and are input to the ring resonator R2.

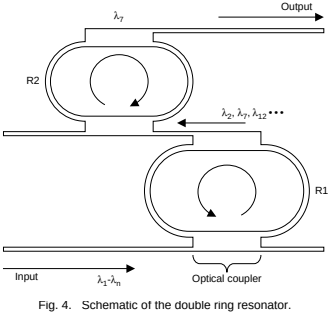

Fig. 4. Schematic of the double ring resonator.

These selected WDM signals are selected again by R2. Thus, the resonant output light, which passes through the double-ring resonator, is only obtained when the resonant frequency of the two single-ring resonators is the same. Thus, the double-ring resonator has a wide tuning range without increasing the tuning range of single resonator. The FSR of double ring resonator is given by

$$FSR = N \cdot FSR_1 = M \cdot FSR_2, \tag{5}$$

where N and M are natural and co-prime numbers and FSR_1 and FSR_2 are the FSRs of R1 and R2 , respectively.

3.3 Calculation of frequency responses

Figure 5 shows the calculated frequency responses. We assumed that the coupling coefficient of the optical coupler, κ, was 0.29, the propagation loss of the ring waveguide was 20 dB/cm, and the FSRs of the ring resonators were 340 and 425 GHz. Thus, N and M in Eq. (5) are 5 and 4. The dashed lines are the calculated optical frequency responses of the single ring resonators. The output from each resonator is a maximum at the resonant frequency. The solid line is the calculated optical frequency response of the double-ring resonator. As shown in this figure, resonant peaks were observed at 0 and 1700 GHz. Spurious resonant peaks, corresponding to the resonant wavelength of either R1 or R2, were also observed. We

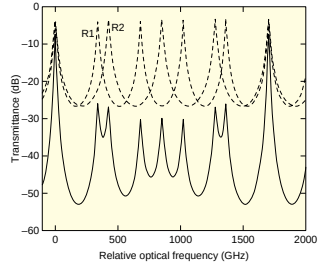

Fig. 5. Calculated frequency responses. Dashed lines are the calculated optical frequency responses of the single ring resonators. The solid line is the calculated optical frequency response of the double-ring resonator.

define the contrast ratio as the power difference between the resonant and spurious resonant peaks. In this calculation, the loss of the device was 7.3 dB and the contrast ratio was 18.6 dB.

3.4 Wavelength tuning

When current is injected into R1 in Fig. 4, the effective refractive index of the waveguide is decreased. Thus, the resonant wavelength of R1 decreases and the resonant frequency correspondingly increases. As a result, the transmission spectrum of R1 in Fig. 5 shifts to the right. The transmissivity of the double ring resonator is the product of the transmissivity of each ring resonator. Thus, the next large transmissivity appeared at 425 GHz in relative optical frequency. In the same way, when the current injection to R1 is increased, a large resonant peak appears at 850 and 1275 GHz. On the other hand, increasing the injection current to R2 produces a large resonant peak at 1360, 1020, 680, and 340 GHz. By changing the refractive indices of both ring resonators simultaneously, we can obtain any desired resonant frequency.

3.5 Device design

The loss and crosstalk of the device are very important in determining the device performance. Figure 6 shows the transmission spectrum near the resonance frequency as a function of the coupling coefficient of the optical coupler. As the coupling coefficient increased, the transmissivity and 3-dB bandwidth increased while the contrast ratio decreased. Thus controlling the coupling coefficient of the optical coupler is very important because the contrast ratio and loss of the ring resonator strongly depend on it.

A suitable way to control the coupling coefficient is to use a directional coupler. However, to obtain a wide tuning range, the FSR of a ring resonator must be large. For example, when we assumed that the maximum effective index change was 0.3%, the wavelength shift was 4.65 nm, which corresponds to an optical frequency range of 580 GHz. In this case, the total waveguide length was about 144 μm and the diameter of the ring waveguide was less than 45.7 μm even if we assumed that the length of optical coupler was zero. Thus, we used a high-mesa waveguide structure to reduce the radiation loss. In this case, the directional coupler needs a small gap of less than 0.1 μm between two high-mesa waveguides to obtain a short optical coupler. The processing to make a 0.1-μm gap, by electron beam lithography and dry etching, has low productivity and reproducibility, so we decided to use a multimode interference (MMI) coupler.

However, controlling the coupling coefficient of the MMI coupler is difficult for a simple small structure. To overcome this problem, we etched a groove in the center of the MMI coupler [9]. Figure 7 shows the coupling coefficient calculated by the beam propagation method (BPM) as a function of the groove depth. For this calculation, we assumed a waveguide consisting of a 0.4-μm-thick InGaAsP (1.3Q) layer sandwiched between the 1.5-μm-thick InP layers. The waveguide and groove widths were 1.8 and 0.8 μm, respectively. The etching depth is defined as 0 μm for etching through the top of the InGaAsP core layer.

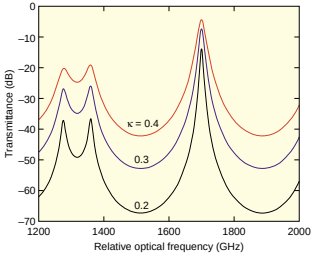

Fig. 6. Transmission spectrum near the resonance frequency as a function of coupling coefficient of the optical coupler.

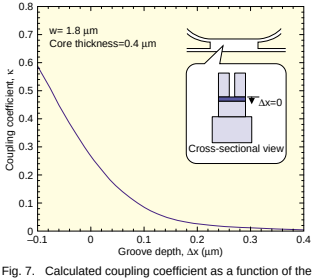

Fig. 7. Calculated coupling coefficient as a function of the groove depth.

The coupling coefficient decreases with increasing groove depth, indicating that the coupling coefficient can be controlled by adjusting the groove depth.

4. Device fabrication and characteristics

Figure 8(a) shows a photograph of the fabricated double-ring resonator, and Fig. 8(b) is a scanning electron microscope image of the ring resonator taken after the dry-etching process. The epitaxial wafer was grown by metalorganic chemical vapor deposition on an n-doped InP substrate. It consisted of a p^+-InGaAs contact layer, a 1.2-μm-thick p-InP cladding layer (doping concentration: 2×10^{17} cm^{-3}), a 0.4-μm-thick InGaAsP layer (1.3Q), and a 0.5-μm-thick n-InP buffer layer. The high-mesa waveguide structure was formed by Br_2-N_2 reactive beam etching [10]. For current injection, Ni/Zn/Au electrodes were deposited on the p^+-InGaAs contact layer. The waveguide width and height were 1.8 and 3.5 μm, respectively. The radii of the ring resonators were 25.2 and 17.8 μm, which correspond to FSRs of 340 and 425 GHz, respectively. The device size was 500×500 μm^2 including the bonding pads.

Figure 9 shows the optical frequency response of the double-ring resonator for transverse electric (TE) polarization. The light source was a tunable laser diode and the current in R1 was set to 1.3 mA. Resonant peaks were observed at 1541.8 and 1555.3 nm. Thus, the total FSR of the double-ring resonator was 13.5 nm, which is approximately 1700 GHz in the frequency domain. Spurious resonant peaks, corresponding to the resonant wavelength of either resonator R1 or R2, were also observed. The crosstalk between the resonant and spurious resonant peaks was 9.5 dB, as determined from the crosstalk of each single-ring resonator.

Figure 10 shows the tuning characteristics of the double-ring resonator. We changed the injection current of R1 from 0 to 6.3 mA while keeping that of R2 constant at 0 mA. The refractive index of the ring waveguide in R1 decreased with increasing injection current, so the resonant wavelength of R1 gradually decreased. As described before, resonant output from the double-ring resonator occurs where both rings have a common resonant wavelength. Thus, resonant outputs were obtained for currents of 0, 1.3, 3.3, and 6.3 mA and they appear every 425 GHz. This is consistent with the FSR of R2.

The dynamic response of the ring resonator is shown in Fig. 11. In this experiment, the device was a single-ring resonator. The current was driven between 0 and 1.8 mA at intervals of 400 ns. In Fig. 11(a), the wavelength of the tunable laser diode was 1550.1 nm, which is the resonant wavelength for injection current of 0 mA. In Fig. 11(b), the wavelength of the tunable laser diode was 1549.1 nm, which is the resonant wavelength for injection current of 1.8 mA. As these figures show, fast and stable switching was achieved by current injection. The

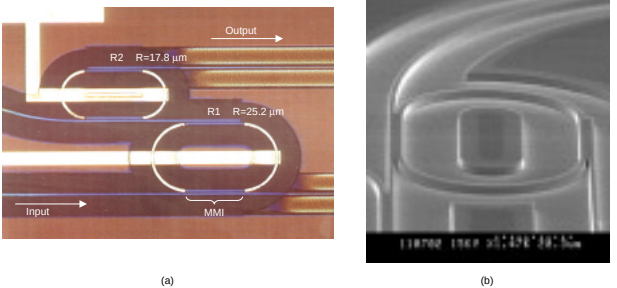

(a) (b)

Fig. 8. (a) Photograph of the fabricated double-ring resonator and (b) SEM image of the ring resonator taken after the dry-etching process.

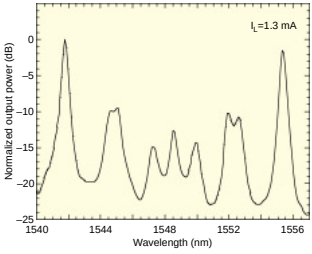

Fig. 9. Optical frequency response of the double-ring resonator for TE polarization.

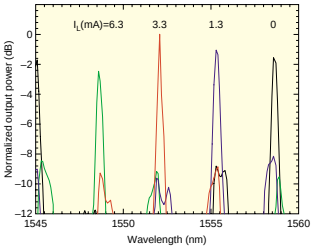

Fig. 10. Tuning characteristics of the double-ring resonator.

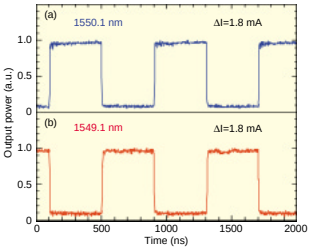

Fig. 11. Dynamic response of the ring resonator.

switching time was 2.5 ns.

5. Discussion

The characteristics of the fabricated device were not as good as the calculated values. As Fig. 12 shows, the calculated transmissivity at the resonant wavelength and the contrast ratio both decreased with increasing MMI coupler loss. When the loss was 1.0 dB, they were –27.0 and 10.4 dB, respectively because the light in the ring resonator passed through the MMI coupler until it reached the output port. Thus, it is important to reduce the MMI coupler loss. In the BPM calculation, the MMI coupler loss was estimated to be as low as 0.2 dB. However, in the fabricated device, the etching width of the center of MMI coupler was increased and this changed the optimal length of the MMI coupler, resulting in higher MMI coupler loss. It should be possible to reduce the MMI coupler loss by optimizing.

Another problem is obtaining a low-cost tunable filter. In general, the semiconductor WDM devices require precise temperature control, which is expensive. An arrayed device, consisting of many tunable optical filters and photodetectors, could solve this problem.

6. Conclusion

We have demonstrated a high-speed tunable optical filter using a semiconductor double-ring resonator. The device shows total FSR of 13.5 nm and contrast

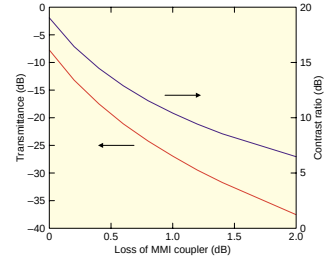

Fig. 12. Calculated transmissivity at the resonant wavelength and contrast ratio as a function of the loss of MMI coupler.

ratio of 9.5 dB between desired and spurious resonant peaks. Its switching time is 2.5 ns. This is the first time a high-speed tunable optical filter has been fabricated using semiconductor ring resonators.

Acknowledgments

We thank Junji Yumoto and Chikara Amano for stimulating discussions, and Kazuaki Ishibashi and Toru Kodaira for device fabrication and measurements.

References

[1] A. Misawa, K. Sasayama, and Y. Yamada, "WDM knockout switch with multi-output-port wavelength-channel selectors," J. Lightwave Technol., Vol. 16, No. 12 , pp. 2212-2219, 1998.

[2] C. Guillemot, M. Renaud, P. Gambini, C. Janz, I. Andonovic, R. Bauknecht, B. Bostica, M. Burzio, F. Callegati, M. Casoni, D. Chiaroni, F. Clerot, S. L. Danielsen, F. Dorgeuille, A. Dupas, A. Franzen, P. B. Hansen, D. K. Hunter, and A. Kloch, "Transparent optical packet switching: the European ACTS KEOPS project approach," J. Lightwave Technol., Vol. 16, No. 12, pp. 2117-2134, 1998.

[3] M. K. Chin, C. Youtsey, W. Zhao, T. Pierson, Z. Ren, S. L. Wu, L. Wang, Y. G. Zhao, and S. T. Ho, "GaAs Microcavity Channel-Dropping Filter Based on a Race-Track Resonator," IEEE Photon. Technol. Lett., Vol. 11, No. 2, pp. 1620-1622, 1999.

[4] Y. Ma, S. H. Chang, S.S. Chang, and S. T. Ho, "Improved optical filter responses in cascaded InGaAsP/InP microdisk resonators," Electron. Lett., Vol. 37, No. 9, pp. 564-565, 2001.

[5] T. Okugawa, T. Matsunaga, and K. Habara, "Composite optical/electrical buffer configuration for photonic ATM switching systems," Electron. Lett., Vol. 33, No. 16, pp.1398-1400, 1997.

[6] H. Ishii, M. Kohtoku, Y. Shibata, S. Oku, Y. Kadota, Y. Yoshikuni, H. Sanjoh, Y. Kondo, and K. Kishi, "Zero insertion loss operations in monolithically integrated WDM channel selectors," IEEE Photon. Technol. Lett., Vol. 11, No. 2, pp. 242-244, 1999.

[7] S. Suzuki, K. Oda, and Y. Hibino, "Integrated-Optic Double-Ring Resonators with Wide Free Spectral Range of 100 GHz," J. Lightwave Technol., Vol. 13, No. 8, pp. 1766-1771, 1995.

[8] S. Matsuo, Y. Ohiso, K. Tateno, T. Segawa, M. Kohtoku, and S. Oku, "A high-speed tunable optical filter using a semiconductor double-ring resonator," IPRM 2002, pp. 467-470, 2002.

[9] G. Griffel, J. H. Abeles, R. J. Menna, A. M. Braun, J. C. Connolly, and M. King, "Low-Threshold InGaAsP Ring Lasers Fabricated Using Bi-Level Dry Etching," IEEE Photon. Technol. Lett., Vol. 12, No. 2, pp. 146-148, 2000.

[10] S. Oku, and Y. Shibata, "Semiconductor photonic waveguide structures made by a reactive beam etching technique," IPRM 2001., pp. 75-78, 2001.

Shinji Matsuo
Senior Research Engineer, Advanced Optoelectronics Laboratory, NTT Photonics Laboratories.
He received the B.E. and M.E. degrees in electrical engineering from Hiroshima University, Hiroshima in 1986 and 1988, respectively. In 1988, he joined NTT Opto-electronics Laboratories, Atsugi, where he was engaged in research on photonic functional devices using MQW-pin modulators and VCSELs. In 1997, he researched optical networks using WDM technologies at NTT Network Innovation Laboratories, Yokosuka. Since 2000, he has been researching a high-speed tunable optical filter and laser for photonic packet switching at NTT Photonics Laboratories, Atsugi. He is a member of Japan Society of Applied Physics and the IEEE Lasers and Electro-Optics Society.

Yoshitaka Ohiso
Senior Research Engineer, Advanced Optoelectronics Laboratory, NTT Photonics Laboratories.
He received the B.E. and M.E. degrees in electrical engineering from Keio University, Yokohama in 1989 and 1991, respectively. Since joining the NTT Laboratories, Kanagawa Japan in 1991, he has been engaged in the research and development of 0.85-μm bottom-emitting VCSELs on an AlGaAs substrate. His current research interests include MOCVD epitaxial growth and device fabrication process techniques for long wavelength VCSELs. He is a member of JSAP and the Institute of Electronics, Information and Communication Engineers of Japan.

Toru Segawa
Researcher, Advanced Opto-electronics Laboratory, NTT Photonics Laboratories.
He received the B.E. and M.E. degrees in electrical engineering from Keio University, Yokohama in 1999 and 2001, respectively. In 2001, he joined NTT Photonics Laboratories and has been working on a high-speed tunable optical filter for photonic packet switching.